

ANALYSIS AND DESIGN OF A RECTANGULAR DIELECTRIC RESONATOR ANTENNA FED BY DIELECTRIC IMAGE LINE THROUGH NARROW SLOTS

A. S. Al-Zoubi, A. A. Kishk, and A. W. Glisson

Department of Electrical Engineering
Center for Applied Electromagnetic System Research
University of Mississippi
University, MS 38677, USA

Abstract—Analysis and design of a narrow aperture coupled rectangular dielectric resonator antenna (DRA) fed by dielectric image line (DIL) are presented. The modal expansion method is used to describe the fields in the dielectric resonator side and the change in the modal voltage of the image line at the aperture is developed to analyze the single element DRA. The DIL is connected to the X-band rectangular waveguide through a waveguide transition and DIL tapering is used to match between the waveguide and the DIL.

1. INTRODUCTION

Dielectric resonator antennas have been developed for use in the microwave and millimeter frequency bands. They have several advantages over microstrip patch antennas such as smaller size, higher radiation efficiency, wider bandwidth, and no excitation of surface waves [1–5]. Previously, the aperture coupled rectangular DRA fed by a microstrip line was analyzed [6]. For high-frequency applications microstrip feed lines have high conductive losses, and very thin substrates are used to avoid direct radiation from the microstrip line and to reduce the surface wave strength. A dielectric image line is an alternate feed method that has lower losses at higher frequencies [7]. In [8] and [9], the aperture-coupled microstrip patch antenna fed by a DIL was analyzed. Good gain, low return loss, and low back radiation were observed.

This paper presents a narrow slot coupled rectangular dielectric resonator antenna fed by a dielectric image line. The modal expansion

method is used to describe the field on the DRA side and the change in the modal voltage of the image line at the narrow slot is developed to analyze the DRA. Only the dominant mode is assumed propagating in the DIL. The slot width is assumed to be narrow compared to the DIL guiding wavelength and the slot length. The electric field in the aperture is assumed to have sinusoidal distribution. The normalized input impedance can be determined from the power and the voltage difference across the slot [10]. The structure has also been analyzed numerically using HFSS [11]. To excite the DIL and define a port, the DIL is connected to an X-band rectangular waveguide through a matching transition. The DIL ends are tapered to achieve smooth transition between the waveguide and the DIL [12, 13].

2. MODAL ANALYSIS FORMULATION

Figure 1 shows the structure of the rectangular DRA fed by the DIL and the coordinate system used in the analysis. The analysis is divided into three parts: analysis of DRA, DIL, and the aperture.

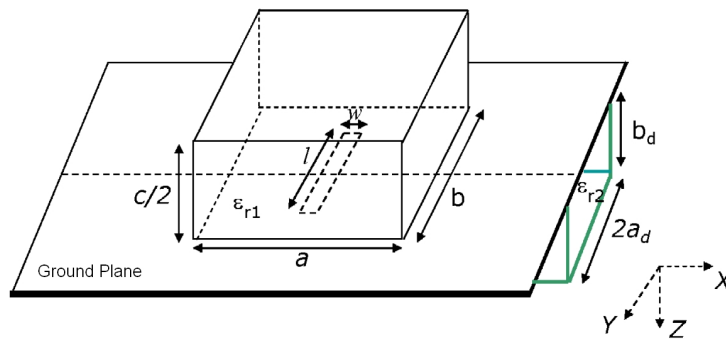


Figure 1. DRA fed by DIL geometry.

2.1. Analysis of the DRA

In the analysis of the DRA side, the modal expansion method is used. To simplify the analysis, the DRA is treated as a dielectric slab inside a waveguide with magnetic conducting walls located at $|x| = a/2$ and $z = -c/2$, and with an electric conducting wall at $z = 0$. The fields are assumed to be standing waves within the dielectric and attenuating outside the dielectric region in the y -direction. Applying the boundary conditions at the walls of the DRA we obtain $k_{x1} = \pi/a$, $k_{z1} = \pi/c$, and k_{y1} from the roots of the following equation $\tan(k_{y1}b/2) = k_{y01}/k_{y1}$,

where $k_{y01}^2 = k_{x1}^2 + k_{z1}^2 - k_0^2$ and $k_{y1}^2 = \varepsilon_{r1}k_0^2 - k_{z1}^2 - k_{x1}^2$. Considering the TE_{111}^y mode, the far field radiation is similar to a magnetic dipole of moment P_m given by:

$$P_m = -\frac{j8A\omega\varepsilon_0(\varepsilon_{r1}-1)}{k_{x1}k_{y1}k_{z1}} \sin(k_{y1}b/2) \quad (1)$$

The power radiated by a magnetic dipole is given by [14]

$$P_r = 10k_0^4 |P_m|^2 \quad (2)$$

from which the radiation Q factor (Q_r) can be determined by $Q_r = \omega_0 W / P_r$, where W is the stored energy in the DRA. In addition to the radiated power, the dielectric dissipated power, P_d , and the conducting power loss, P_c , are computed using the following equations

$$P_d = \frac{1}{2} \omega_0 \varepsilon_1 \tan \delta \int_{-a/2}^{a/2} \int_{-b/2}^{b/2} \int_0^{c/2} |\vec{E}|^2 dz dy dx = \omega_0 W \tan \delta \quad (3)$$

$$P_c = \frac{1}{2} \sqrt{\frac{\omega_0 \mu_0}{2\sigma_c}} \left[\int_{-a/2}^{a/2} \left[\int_{-\infty}^{-b/2} |H_0|^2 dy + \int_{-b/2}^{b/2} |H_d|^2 dy + \int_{b/2}^{\infty} |H_0|^2 dy \right] dx - \int_{-w/2}^{w/2} \int_{-l/2}^{l/2} |H|^2 dy dx \right] \quad (4)$$

where $\tan \delta$ is the loss tangent of the dielectric used for the DRA and σ_c is the conductivity of the ground plane. H_0 is the magnetic field outside the DRA, and H_d is the field inside the DRA. The total Q factor is determined by:

$$\frac{1}{Q} = \frac{1}{Q_r} + \frac{1}{Q_d} + \frac{1}{Q_c} = \frac{1}{\omega_0 W} (P_r + P_d + P_c) \quad (5)$$

and the radiation efficiency η is :

$$\eta = Q / Q_r \quad (6)$$

The field in the DRA is normalized such that

$$\int_{-a/2}^{a/2} \int_{-b/2}^{b/2} \int_0^{c/2} \mu_0 (|H_{y111}|^2) dz dy dx = 1.0 \quad (7)$$

2.2. Analysis of the DIL

The DIL supports the TM_{mn}^z and TM_{mn}^y modes. However, the presence of the ground plane resolves the degeneracy because the strongest electric field component of the TM_{11}^y mode is shorted out, so only the TM_{11}^z mode is attained over the desirable frequency range. It is not possible to have a closed form solution for the DIL problem since it is an open structure that does not fit the rectangular coordinate system in a straight forward manner. However, it is possible to simplify the problem by considering infinitely long dielectric slabs having effective dielectric constant that can be obtained using the effective dielectric constant (EDC) method [15].

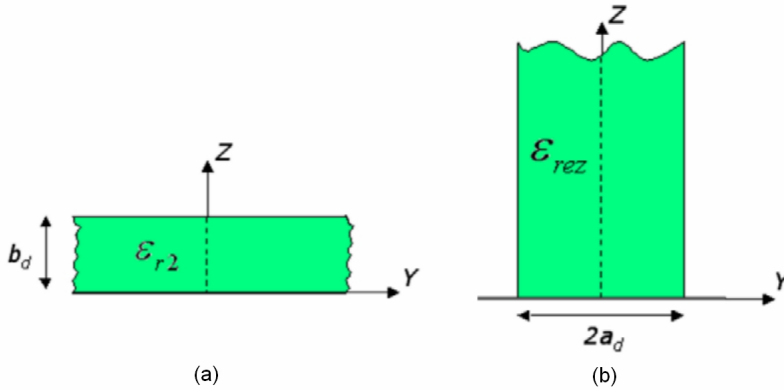


Figure 2. Simplified geometry of the dielectric image guide.

Considering an infinite dielectric slab above a ground plane with height b_d as shown in Fig. 2(a), the continuity of E_y and H_x at $z = b_d$ is enforced and the following equation is obtained:

$$\tan(k_z b_d) = (k_{z0}/k_z) \epsilon_{r2} \quad (8)$$

where $k_{z0}^2 = k_0^2 [\epsilon_{r2} - 1] - k_z^2$, and $k_x^2 = \beta^2 = \epsilon_{r2} k_0^2 - k_z^2 - k_y^2$. The other problem is a dielectric slab that extends infinitely in the z -direction in the upper half-space as shown in Fig. 2(b). When the continuity of E_z and H_x are applied at $y = \pm a_d$, one can obtain

$$\tan(k_y a_d) = \frac{k_{y0}}{k_y} \frac{k_y^2 + k_x^2}{-k_{y0}^2 + k_x^2 \epsilon_{rez}} = \frac{k_{y0}}{k_y} \quad (9)$$

where $\epsilon_{rez} = \epsilon_{r2} - (k_z/k_0)^2$, $k_{y0}^2 = k_0^2 [\epsilon_{rez} - 1] - k_y^2$, and $k_y^2 = \epsilon_{rez} k_0^2 - \beta^2$.

In (8) and (9), k_z, k_y, k_{z0} , and k_{y0} are the transverse propagation constants inside and outside the dielectric slab, respectively. The wave impedance of the image line is given by

$$Z_w = -\frac{E_z}{H_y} = \frac{-k_{y0}^2 + k_x^2}{\omega \varepsilon_0 k_x} = \frac{k_y^2 + k_x^2}{\omega \varepsilon_0 \varepsilon_{rez} k_x} \quad (10)$$

The characteristic impedance, dielectric attenuation constant, and conductor attenuation constant of the image line can be found in [12].

2.3. Analysis of the Aperture

The aperture determines the amount of power coupled from the DIL to the DRA. The slot aperture is centered at the origin with length l and width w . The electric field in the aperture is assumed to be of sinusoidal distribution in the y -direction and independent of x as described by the following equation:

$$E_{ap}^x = \frac{E_0 \sin [K (l/2 - |y|)]}{\sin [Kl/2]} \quad (11)$$

where $K = (2\pi/\lambda_0) \sqrt{(\varepsilon_{r1e} + \varepsilon_{r2})/2}$. The equivalent magnetic current on the slot is given by

$$\vec{M} = E_{ap}^x \hat{x} \times \hat{z} = \hat{y} \frac{E_0 \sin [K (l/2 - |y|)]}{\sin [Kl/2]} = M_y \hat{y} \quad (12)$$

The magnetic current excites only TE^y modes of the DRA. The fields can be expressed in terms of these resonant modes. However, we only considered the TE_{111}^y mode, hence the single mode approximation can be taken. The magnetic field (using modal expansion) is given by:

$$\vec{H} = \sum_i \frac{j\omega H_i}{(\omega^2 - \omega_i^2)} \iiint_v \vec{M} \cdot \vec{H}_i^* dv \quad (13)$$

and for TE_{111}^y mode we have

$$H_y = \frac{j\omega H_{y111}}{(\omega^2 - \omega_{111}^2)} \int_{-w/2}^{w/2} \int_{-l/2}^{l/2} M_y H_{y111} dy dx \quad (14)$$

where $\omega_{111}^2 = \frac{1}{\mu_0 \varepsilon} (k_{x1}^2 + k_{y1}^2 + k_{z1}^2)$, $\varepsilon = \varepsilon_0 \varepsilon_{r1} (1 - j/Q)$, $k_{x1} = \pi/a$, and $k_{z1} = \pi/c$. K_{y1} can be obtained from the roots of the characteristic equation $\tan\left(\frac{k_{y1} b_e}{2}\right) = \frac{k_{y0}}{k_{y1}}$, where $k_{y0}^2 = (\varepsilon_{r1} - 1)k_0^2 - k_{y1}^2$.

The other field components can be derived from H_y using the electric and magnetic vector potentials [16].

The power at the aperture is defined as

$$P = \int_{-w/2}^{w/2} \int_{-l/2}^{l/2} (E_{ap}^x \hat{x} \times H_y \hat{x}) \cdot d\vec{s} = \frac{j\omega \Re^2}{(\omega^2 - \omega_{111}^2)} \quad (15)$$

where

$$\begin{aligned} \Re &= \int_{-w/2}^{w/2} \int_{-l/2}^{l/2} M_y H_{y111} dy dx \\ &= \frac{-j8A (k_{x1}^2 + k_{z1}^2) 2K \sin(wk_{x1}/2)}{\omega \mu_0 \sin[Kl/2] k_{x1} K^2 - k_{y1}^2} \\ &\quad \cdot \left[\sin\left(\frac{K + k_{y1}}{l/4}\right) \cdot \sin\left(\frac{K - k_{y1}}{l/4}\right) \right] \end{aligned} \quad (16)$$

For the fundamental TM_{11}^z mode of the DIL, the electric field in the z -direction and the magnetic field in the y -direction inside the DIL are given by:

$$E_z^d = E^d \cos(k_y y) \cos(k_z z) \quad (17)$$

$$H_y^d = -\frac{\omega \varepsilon_0 \varepsilon_r 2e k_z}{k_x^2 + k_z^2} |E_z^d| \equiv -N |E_z^d| \quad (18)$$

The discontinuity in the voltage across the slot is given by

$$\Delta V = \iint_{slot} (\hat{n} \times E_{ap}^x \hat{y}) \cdot \vec{h}^d ds = \iint_{slot} |E_{ap}^x| |h_y^d| dx dy \quad (19)$$

where \vec{h}^d and \vec{h}_y^d are the normalized magnetic fields in the DIL. The power P_x in the DIL is normalized such that

$$P_x = \int_0^\infty \int_{-\infty}^\infty (\vec{E} \times \vec{H}^*) \cdot \hat{x} dy dz = 1 \quad (20)$$

This determines the constant E_0 in (11). The voltage variation across the slot is expressed by

$$\Delta V = \frac{-8NE_0}{\sin(Kl/2)} \frac{2K \sin(k_x w/2)}{k_x (K^2 - k_y^2)} \cdot \left[\sin\left(\frac{K + k_y}{l/4}\right) \cdot \sin\left(\frac{K - k_y}{l/4}\right) \right] \quad (21)$$

The normalized impedance presented at the aperture is given as

$$z_{ap} = (\Delta V)^2 / P \quad (22)$$

The normalized input impedance depends on the aperture size and DRA size. The reflection coefficient at the aperture is given by [10],

$$R = \frac{1}{2} \iint_{slot} E_{ap}^x(x, y) h_y^d(x, y) ds \quad (23)$$

3. RESULTS AND DISCUSSION

The DRA structure shown in Fig. 1 is analyzed with $a = 6.2$ mm, $b = 6.0$, $c/2 = 6.1$ mm, and $\varepsilon_{r1} = 10.2$. The resonant frequency, radiation Q factor, and radiation efficiency for the DRA are verified with the results available in literature. Using HFSS software, the resonant frequency is 10.0 GHz, and $Q_r = 7.68$. The results obtained for the free space to guide wavelength ratio of the DIL as a function of the normalized height $B = 4b_d\sqrt{\varepsilon_r - 1}/\lambda_0$, are identical to the results obtained in [12]. These results are omitted for brevity. In order to verify these analyses, the reflection coefficient is computed using the present method and using HFSS commercial software [11]. The results are shown in Fig. 3. It can be seen that the results obtained using

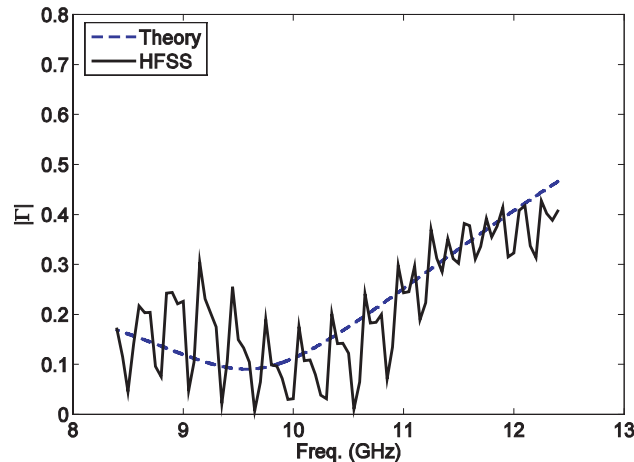


Figure 3. Reflection coefficient at the slot for the DRA-DIL geometry. $W = 0.15$ mm, $L = 4$ mm, $a = 6.2$ mm, $b = 6.0$ mm, $c = 12.2$ mm, $\varepsilon_{r1} = 10.2$, $a_d = 4.5$ mm, $b_d = 4.03$ mm, $\varepsilon_{r2} = 10.2$.

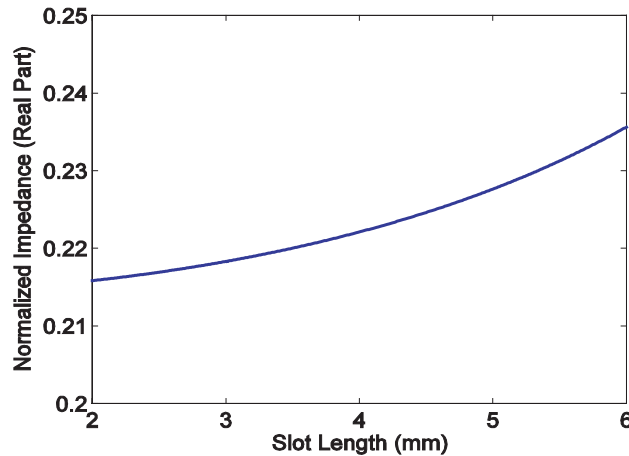


Figure 4. Real part of the normalized impedance as a function of slot length. $W = 0.15$ mm, $a = 6.2$ mm, $b = 6.0$ mm, $c = 12.2$ mm, $\varepsilon_{r1} = 10.2$, $a_d = 4.5$ mm, $b_d = 4.03$ mm, $\varepsilon_{r2} = 10.2$.

HFSS are oscillating as compared with the analytical results. One may relate that to the finite size of the structure and the matching transition used in the numerical model as compared to the infinite size of the analytical model.

Figure 4 shows the real part of z_{ap} of the DRA as a function of the slot aperture length. The variation is approximately linear, and the impedance increases as the slot aperture length increases. The variation of the input admittance versus frequency is shown in Fig. 5.

In order to excite the DIL, the DIL is connected to an X-band rectangular waveguide by means of a three-section transition [12, 13]. The transmission coefficient for the DIL side is shown in Fig. 6. From the figure it can be seen that the system with the transitions and a 16-wavelength long DIL at 10 GHz has a total insertion loss of about 1.5 dB. The radiation patterns in both the E-plane ($\phi = 0^\circ$) and H-plane ($\phi = 90^\circ$) are shown in Fig. 7(a) and 7(b). Fig. 7(a) shows the comparison between computed and simulated radiation patterns with WIPL-D commercial software [17] assuming an infinite ground plane. The results are in good agreement. The computed radiation patterns are obtained by evaluating the electric and magnetic currents at the surfaces of the DRA and its image, and using the formulations in [16]. A comparison of the radiation patterns for the geometry with finite ground plane is shown in Fig. 7(b). The results are obtained using HFSS and WIPL-D, which are commercial software packages based on the finite-element method and the method of moments,

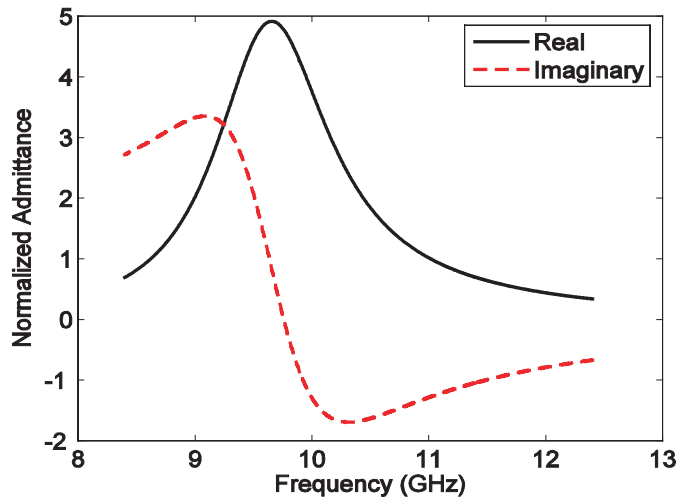


Figure 5. Normalized input admittance as a function of frequency.

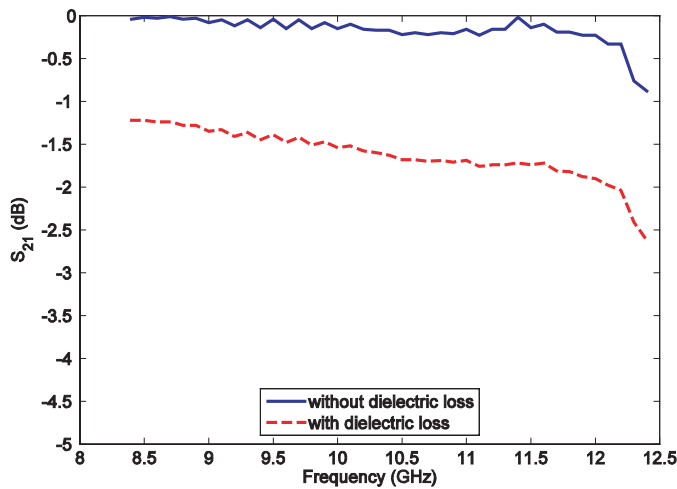


Figure 6. Transmission coefficient of the DIL excited by rectangular waveguide.

respectively. The ripples in the patterns, especially in the E-plane are due to diffraction from the edge of the finite ground plane. The E-plane peak value of the directivity is about 7 dB. The return loss of a single element DRA is shown in Fig. 7(c).

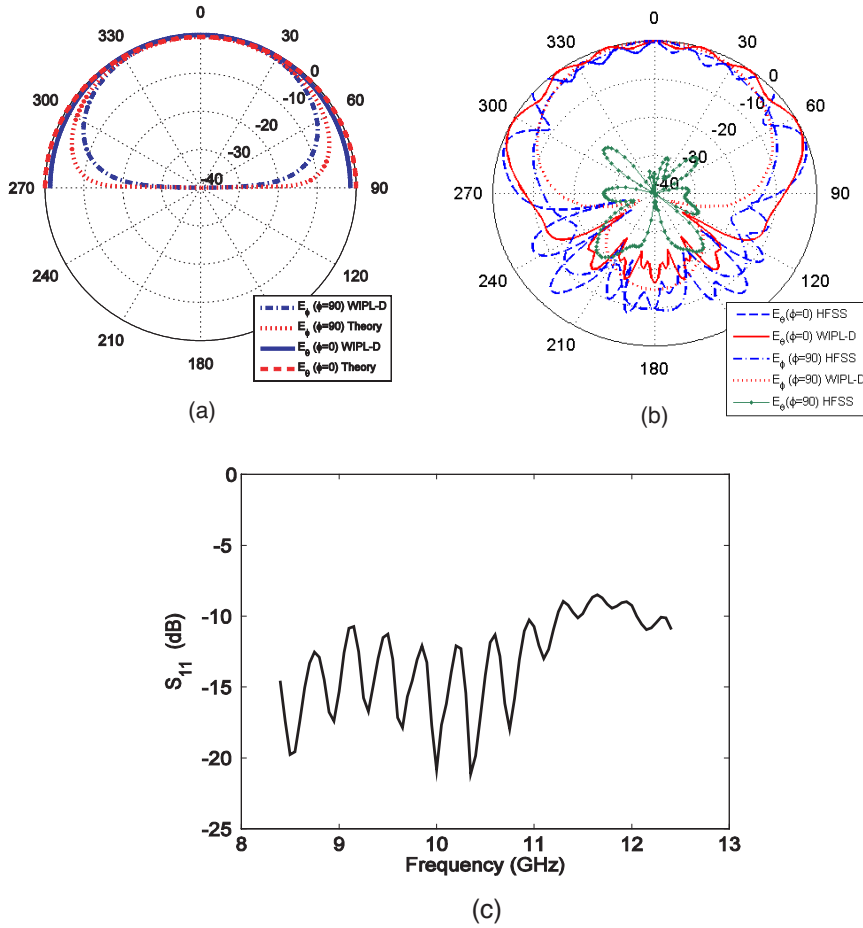


Figure 7. Radiation patterns for (a) infinite ground plane and (b) finite ground plane; (c) return loss for a single element DRA.

4. CONCLUSION

A dielectric resonator coupled to a dielectric image line through a narrow slot was analyzed. The approach combined the modal expansion method on the DRA side and the change in the modal voltage of the image line at the aperture to analyze the single element DRA. The results for Q-factor, resonant frequency, and radiation efficiency of the DRA were verified. Also, the free space to guide wavelength ratio for the dielectric image line as a function of the

normalized height were found to be in good agreement with the results available in the literature. The reflection coefficient at the slot was verified with HFSS. A good return loss is obtained for a single element DRA. The E-plane peak value of the directivity is about 7 dB.

REFERENCES

1. Kishk, A. A., "Dielectric resonator antenna, a candidate for radar applications," *Proceedings of 2003 IEEE Radar Conference*, 258–264, May 2003.
2. Shin, J., A. A. Kishk, and A. W. Glisson, "Analysis of rectangular dielectric resonator antennas excited through a slot over a finite ground plane," *IEEE AP-S International Symposium*, Vol. 4, 2076–2079, July 2000.
3. Coulibaly, Y. and T. A. Denidni, "Design of a broadband hybrid dielectric resonator antenna for X-band applications," *J. of Electromagn. Waves and Appl.*, Vol. 20, No. 12, 1629–1642, 2006.
4. Fayad, H. and P. Record, "Multi-feed dielectric resonator antenna with reconfigurable radiation pattern," *Progress In Electromagnetics Research*, PIER 76, 341–356, 2007.
5. Rezaei, M., M. Hakkak, and K. Forooghi, "Design of wide-band dielectric resonator antenna with a two-segment structure," *Progress In Electromagnetics Research*, PIER 66, 111–124, 2006.
6. Antar, Y. M. M. and Z. Fan, "Theoretical investigation of aperture-coupled rectangular dielectric resonator antenna," *IEE Proc. - Antennas Propag.*, Vol. 143, No. 2, 113–118, April 1996.
7. Yau, D. and N. V. Shuley, "Numerical analysis of coupling between Dielectric image guide and microstrip," *J. of Electromagn. Waves and Appl.*, Vol. 20, No. 15, 2215–2230, 2006.
8. Kanamaluru, S., M. Y. Li, and K. Chang, "Aperture coupled microstrip antenna with image line feed," *IEEE AP-S Symp. Dig.*, Vol. 2, 1186–1189, 1994.
9. Kanamaluru, S., M. Li, and K. Chang, "Analysis and design of aperture coupled microstrip patch antennas and arrays fed by dielectric image line," *IEEE Transactions on Antennas and Propagation*, Vol. 44, No. 7, 964–974, July 1996.
10. Pozar, D., "A reciprocity method of analysis for printed slot and slot-coupled microstrip antennas," *IEEE Transactions on Antennas and Propagation*, Vol. 34, No. 12, 1439–1446, 1986.
11. HFSS: *High Frequency Structure Simulator Based on Finite Element Method*, v. 9.2.1, Ansoft Corporation, 2004.

12. Bhartia, P. and I. J. Bahl, *Millimeter-Wave Engineering and Applications*, Wiley, New York, 1984.
13. Dydyk, M., "Image guide: A promising medium for EHF circuits," *Microwaves*, 71–80, April 1981.
14. Mongia, R. K. and A. Ittipiboon, "Theoretical and experimental investigations on rectangular dielectric resonator antennas," *IEEE Transactions on Antennas and Propagation*, Vol. 45, No. 9, 1348–1356, Sept. 1997.
15. Knox, R. M. and P. P. Toullos, "Integrated circuits for the millimeter through optical frequency range," *Proc. Symp. Submillimeter Waves*, 497–516, 1970.
16. Balanis, C. A., *Advanced Engineering Electromagnetics*, Wiley, New York, 1989.
17. Kolundzija, B. M., J. S. Ognjanovic, and T. K. Sarkar, *WIPL-D: Electromagnetic Modeling of Composite Metallic and Dielectric Structures, Software and User's Manual*, Artech House, Reading, MA, 2000.